PCCP

Accepted Manuscript

ROYAL SOCIETY OF CHEMISTRY

www.rsc.org/pccp

Physical Chemistry Chemical Physics: Article

Pentaglyme-K Salt Binary Mixtures: Phase Behavior, Solvate Structures, and Physicochemical Properties

Toshihiko Mandai,[†,Ⅱ,*] *Seiji Tsuzuki,*[‡] *Kazuhide Ueno,*[†] *Kaoru Dokko,*[†,§] *and Masayoshi Watanabe*[†,*]

[†]Department of Chemistry and Biotechnology, Yokohama National University,

79-5 Tokiwadai, Hodogaya-ku, Yokohama 240-8501, Japan

[‡]National Institute of Advanced Industrial Science and Technology (AIST),

Tsukuba Central 2, Tsukuba, Ibaraki 305-8568, Japan

[§]Unit of Elements Strategy Initiative for Catalysts & Batteries (ESICB), Kyoto University,

Kyoto 615-8510, Japan

[Ⅱ]Department of Applied Physics, Chalmers University of Technology

Göteborg, SE-412 96, Sweden

AUTHOR EMAIL ADDRESS: mandi@chalmers.se mwatanab@ynu.ac.jp

RECEIVED DATE (to be automatically inserted after your manuscript is accepted if required according to the journal that you are submitting your paper to)

ABSTRACT. We prepared a series of binary mixtures composed of certain K salts (KX) and pentaglyme (G5) with different salt concentrations and anionic species ($[X]^-$: $[(CF_3SO_2)_2N]^-$ = $[TFSA]^-$, $[CF_3SO_3]^-$ = $[TfO]^-$, $[C_4F_9SO_3]^-$ = $[NfO]^-$, PF_6^-, SCN^-), and characterized them with respect to their phase diagrams, solvate structures, and physicochemical properties. Their phase diagrams and thermal stability strongly implied the formation of equimolar complexes. Single-crystal X-ray crystallography was performed on certain equimolar complexes, which revealed that G5 molecules coordinate to K^+ cations in a characteristic manner, like 18-crown-6 ether in the crystalline state, irrespective of the paired anions. The solvate structures in the molten state were elucidated by a combination of temperature-dependent Raman spectroscopy and X-ray crystallography. A drastic spectral variation was observed in the $[K(G5)_1][TfO]$ Raman spectra, indicating that solvate structures in the crystalline state break apart upon melting. The solvate stability of $[K(G5)_1]X$ is closely related to the ion–ion interaction of the parent salts. A stable solvate forms when the ion–dipole interaction between K^+ and G5 overwhelms the ion–ion interaction between K^+ and X^-. Furthermore, the physicochemical properties of certain equimolar mixtures were evaluated. A Walden plot clearly reflects the ionic nature of the molten equimolar complexes. Judging from the structural characteristics and dissociativity, we classified $[K(G5)_1]X$ into two groups, good and poor solvate ionic liquids.

KEYWORDS: solvate ionic liquids, glyme-K salt binary mixtures, solvate structures, physicochemical properties

1. INTRODUCTION

Recently, the subclasses of ionic liquids (ILs) has gradually broadened owing to the emergence of various characteristic IL analogs.[1–9] They possess rather remarkable features which makes understanding these complicated systems important. Among them, solvate ILs are a particularly significant class because of their potential for widespread application.[9–17] The term "solvate ILs" was first proposed by Angell according to the following definition: ILs where ligand molecules, as a third component, strongly coordinate to the cations and/or anions, thereby forming robust complex ions.[18] Because solvate ILs can involve various metal cations as component ions by complexation of salts with appropriate ligands, they are promising substances in diverse areas of materials science.

One of the representative solvate ILs is glyme-Li salt equimolar complexes. We have reported that equimolar mixtures of certain Li salts and glymes ($CH_3O(CH_2CH_2O)_nCH_3$) are in the liquid state at ambient temperature and behave like typical aprotic ionic liquids.[8,9,19] Systematic studies on the glyme-Li salt mixtures identified their characteristic features. Complexation of Li^+ ions with glymes considerably enhances their oxidative and thermal stability, and results in anomalous solubility.[8,9,12,13,20] The ionic nature of the equimolar mixtures is dominated by the Lewis basicity of the paired anion species.[21] Glyme length also significantly impacts the solvate stability of complex cations in the electrolyte.[22,23] These studies, and subdivision of solvate ILs based on their structural stability, are summarized in our recent perspective article.[24] Many researchers have also reported the fundamental properties and possible applications of solvate ILs. Brouillette's and Henderson's groups previously performed pioneering work on the phase diagrams and solvate structures of a series of glyme-Li salt mixtures.[25–30] Theoretical calculations of equimolar glyme-alkali metal salts have been performed to obtain stable solvate structures.[31,32] Bruce et al. reported the selective ion transport behavior in glyme-$LiAsF_6$ complex-based solid electrolytes.[33,34] The first use of glyme-Li solvate ILs was as an alternative electrolyte for Li-secondary batteries. Owing to their remarkable properties mentioned above, solvate

ILs have proved to be fascinating electrolytes in Li-secondary batteries with a variety of cathodic and anodic materials.[10–13,35,36]

On the basis of the similarity of the chemical nature among congeners, an appropriate combination of glymes and other alkali-metal salts should potentially form solvate ILs. Previously, we revealed that certain equimolar mixtures, composed of appropriate glyme and alkali metal salt paired with the $[TFSA]^-$ anion, can be classified as solvate ILs.[23] Glyme-Li and glyme-Na systems with equimolar mixtures of ClO_4^- or other imide anions can also be referred to as solvate ILs.[21,37] However, the border for the K-glyme system is still unambiguous. To this end, we herein studied a series of glyme-K salt binary mixtures with respect to their phase diagrams, solvate structures, and physicochemical properties. A variety of K salts paired with different anions, such as bis(trifluoromethanesulfonyl)amide ($[(CF_3SO_2)_2N]^-$ = $[TFSA]^-$), trifluoromethanesulfonate ($[CF_3SO_3]^-$ = $[TfO]^-$), nonafluorobutanesulfonate ($[C_4F_9SO_3]^-$ = $[NfO]^-$), hexafluorophosphate (PF_6^-), and thiocyanate (SCN^-), were selected as the parent salts to investigate the anionic (Lewis basicity) effect on the characteristics of the complexes. On the basis of the preferential coordination number and high affinity of 18-crown-6 ether with K^+ cations,[38–41] these K salts were complexed with pentaglyme (G5), in which six oxygen atoms are involved within a single molecule, hereafter abbreviated as $[K(G5)_n]X$ based on the molar ratio of the K salt and G5.

Phase diagrams provide significant information about the binary mixtures that form complexes at certain molar ratios. From these diagrams, the stable complex compositions were examined. The solvate structures of the 1:1 complexes, $[K(G5)_1]X$, in the crystalline state were revealed by single-crystal X-ray structure analyses. By comparison with the solvate structures with different cationic and anionic components, the correlation between the solvate structures and the constituents of the complexes was elucidated. With the results of X-ray structure analyses and the Raman spectra, the "liquid state" solvate structure and the coordination structure of the mixtures and 1:1 complexes were examined. Furthermore, various liquid properties of equimolar liquid molten mixtures were investigated. Based on the structural

characteristics and physicochemical properties, we considered whether a series of $[K(G5)_1]X$ can be categorized as solvate ILs.

2. EXPERIMENTAL SECTION

Materials. K[TFSA], K[TfO], K[NfO], KPF_6, KSCN, and 18-crown-6 ether were purchased from Wako Chemical. All the K-salts were dried under high vacuum at 80 ºC for 36 h, and stored in an Ar-filled glove box before use. G5 was supplied by Nippon Nyukazai and used as received. The residual water content in G5 measured by Karl-Fischer titration was less than 30 ppm. A series of G5-K salt binary mixtures $[K(G5)_n]X$, with molar ratios in the range n = 0.8–9 (mole fraction x = 0.10–0.55), were prepared by mixing stoichiometric K salts and G5 in the Ar-filled glove box. The mixtures were heated to 60 ºC and stirred for 24 h to achieve complete mixing. Equimolar mixtures consisting of 18-crown-6 ether and K salts, abbreviated as $[K(18C6)_1]X$, were also obtained by mixing appropriate quantities of each in the glove box. Owing to the high melting point of the resulting complexes, these crown-ether based complexes were prepared by addition of parent salts into the 18-crown-6 ether/acetone solution, followed by solvent removal under vacuum.

Measurements. The thermal properties such as melting point (T_m), solid-solid transition temperature (T_{tr}), glass transition temperature (T_g), and other thermal transition temperature (T_x), were determined by differential scanning calorimetry (DSC; DSC6220 or DSC7020, Seiko). The samples were hermetically sealed in aluminum pans in the glove box. The samples were scanned under a nitrogen atmosphere at a heating rate of 5 or 10 ºC min^{-1} over a temperature range from −100 to 100 ºC. The sample pans were cooled/annealed repeatedly to achieve complete crystallization of the complexes. The peak tops of the endothermic peaks were taken as T_m, T_{tr}, and T_x. The onset in heat capacity change was taken as T_g. To estimate the temperature dependent thermal stability of the mixtures, a thermogravimetry (TG) measurement was performed with a TG/TDA 6200 (Seiko) from room temperature to 500 ºC at a heating rate of 10 ºC min^{-1} under a nitrogen atmosphere. The thermal decomposition temperature (T_d)

was defined as the temperature at 5% loss of weight. For the 1:1 mixtures, the temperature dependences of the liquid density, viscosity, and ionic conductivity were estimated in the temperature range of 40–80 ºC. The liquid density and viscosity were determined using a SVM3000 (Anton Paar). The ionic conductivity was measured using the complex impedance method in the frequency range of 13×10^6–5 Hz with a sinusoidal alternating voltage amplitude of 10 mV root-mean-square (rms) (4192A, Hewlett Packard). The cell constants for the lab-made cells with two platinum black electrodes were determined in a 0.01 M KCl aqueous solution at 25 ºC. The platinum black electrodes were dipped in the mixture, and the sample cell was thermally equilibrated at each temperature for at least 60 min using a thermostat chamber.

Raman spectra measured with a portable Raman system (RMP-330, Jasco) were excited by a 532 nm solid-state laser. The resolution of the apparatus was ca. 2 cm^{-1}. Raman spectra of all mixtures were measured in the range of 1570 to 370 cm^{-1} at ambient temperature (22±2 ºC). For equimolar complexes, $[K(G5)_1]X$, Raman spectra at 20, 50, and 80 ºC were collected using a hot stage with a temperature controller (mK1000, Instec) to examine the coordination environment of the complexes in the liquid state. All Raman spectral bands were analyzed for different compositions at different temperatures, and suitable spectra ranges were used to analyze the variation of the Raman shift and wave shape attributed to representative vibrational modes of each component:[30,42–51] glyme, from 900 to 780 cm^{-1}; [TFSA], from 760 to 720 cm^{-1}; [TfO], from 1060 to 1000 cm^{-1}; [NfO], from 1040 to 1000 cm^{-1}; PF_6, from 760 to 720 cm^{-1}; and SCN, from 770 to 710 cm^{-1}.

Suitable crystals of $[K(G5)_1][TfO]$, $[K(18C6)_1][TfO]$, $[K(18C6)_1]PF_6$, and $[K(18C6)_1]SCN$ for single-crystal X-ray diffraction were obtained by slow condensation of dilute solutions. The crystallization conditions have almost no effect on the resulting crystal structures. Each single crystal was mounted on a glass pin coated with a minimal amount of perfluoro ether oil to avoid adsorbing moisture and cooled to −100 ºC by a stream of nitrogen gas. Crystal evaluations and data collections were performed with a Rigaku Mercury70 diffractometer using graphite monochromated Mo-Kα radiation. The structures were solved by direct methods SIR92[52] and refined by full-matrix least-squares SHELXL-97.[53,54] Non-

hydrogen atoms were refined anisotropically, and hydrogen atoms were included in their ideal positions. All calculations were performed using the crystallographic software package.[55]

Calculations. The Gaussian 03 program[56] was used for the *ab initio* molecular orbital calculations. The geometries of ion pairs were fully optimized at the HF/6-311G** level. The intermolecular interaction energies (E_{int}) were calculated at the MP2/6-311G** level by the supermolecule method.[57,58] The basis set superposition error (BSSE)[59] was corrected for all the interaction energy calculations using the counterpoise method.[60] The stabilization energy for the formation of ion pairs from isolated ions (E_{form}) was calculated as the sum of E_{int} and the deformation energy (E_{def}), which is the increase of energy of anions by deformation of the geometry associated with the ion pair formation.[61] The E_{def} was calculated at the MP2/6-311G** level.

3. RESULTS AND DISCUSSION

3.1 Phase diagrams and thermal properties

Phase diagrams: **Figure 1** illustrates the phase diagrams for the binary mixtures of G5 and a series of K salts with $[TFSA]^-$, $[TfO]^-$, $[NfO]^-$, PF_6^-, and SCN^- anions. The diagram for G5-K[TFSA] is reproduced from ref. 23. Except for the G5-KPF_6 systems, the diagrams showed similar patterns. The T_m minima appeared at KX mole fractions of x = 0.1–0.25 (n = 9–3). Further addition of K salts into the mixtures elevates T_m, and consequently, T_m reached a maximum at 1:1 composition. These results strongly suggest the formation of 1:1 complexes $[K(G5)_1]X$. For the mixtures with $[TFSA]^-$, $[NfO]^-$, and SCN^- anions, only the T_g was observed in the composition range of x = 0.25–0.4 (n = 3–1.5), the so-called crystallinity gap. It is well known that $[TFSA]^-$ and $[NfO]^-$ anions can possess diverse conformations[62,63] and an SCN^- anion can coordinate to a K^+ cation in the thiocyanate (K–SCN) and isothiocyanate (K–NCS) forms.[51] These anionic structural aspects probably prevent mixtures from crystallizing.

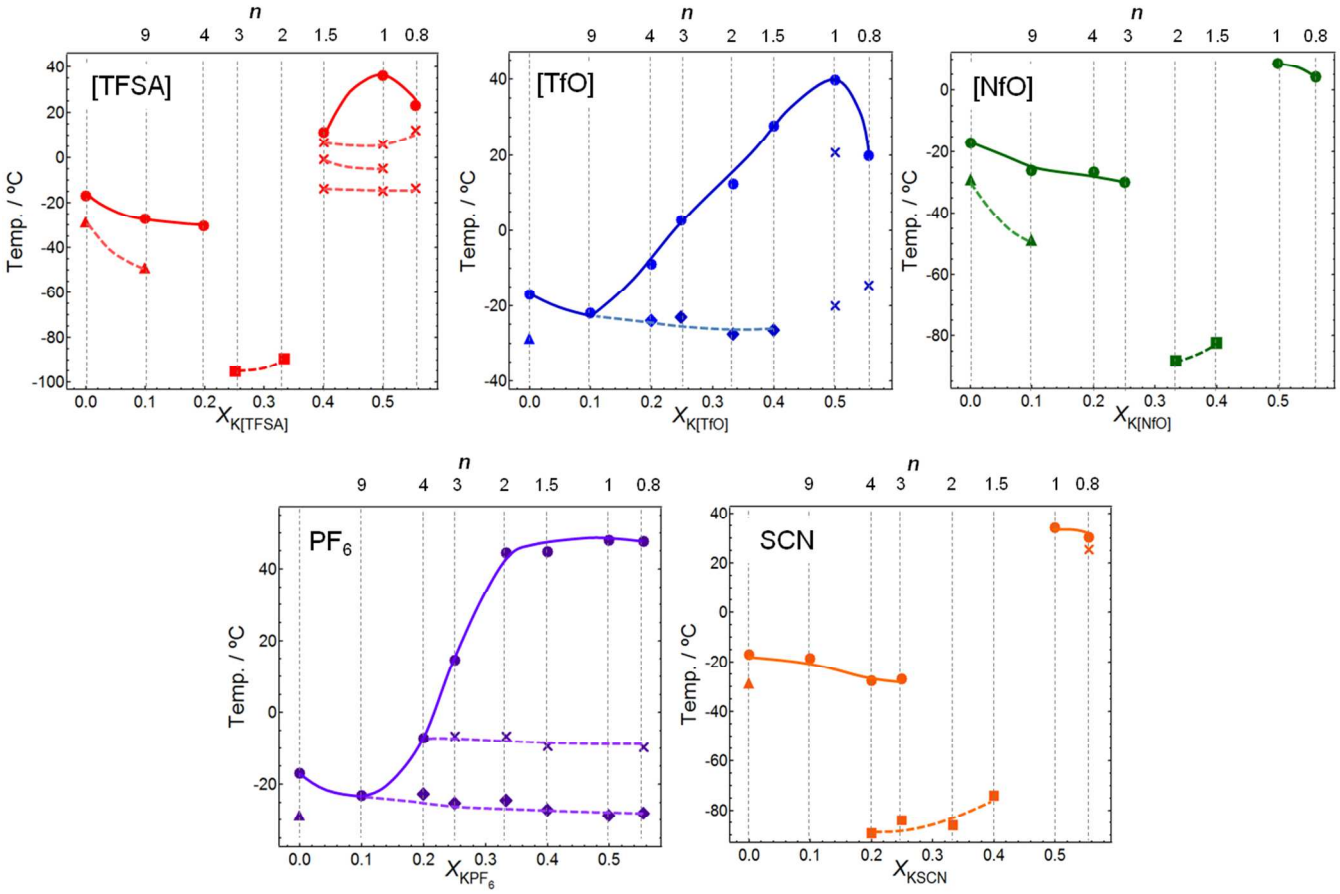

Figure 1. Phase diagrams of $[K(G5)_n]X$ paired with $[TFSA]^-$, $[TfO]^-$, $[NfO]^-$, PF_6^-, and SCN^- anions as a function of mole fraction of K salts. The symbols in the figure indicate T_m (closed circles), T_{tr} (closed triangles), T_g (closed squares), and T_x (closed argyles, crosses). Solid and dotted lines are a guide to the eye.

As shown in the DSC curves (**Figure S1**), the peaks observed before melting for pure G5, $[K(G5)_9][TFSA]$, and $[K(G5)_9][NfO]$ were probably due to the solid-solid transition (T_{tr}) of G5. For the $[K(G5)_n][TFSA]$ system, some endothermic peaks were observed at −15, −5, and 5 ºC before melting in the range of x = 0.4–0.55 (n = 1.5–0.8). These peaks were largest in the $[K(G5)_1][TFSA]$, suggesting that they arise from certain thermal events related to the phase transition of $[K(G5)_1][TFSA]$. The DSC measurements were performed repeatedly on these samples, and the results were reproducible. As illustrated in **Figure 1**, the G5-KPF_6 binary mixtures show a peculiar diagram distinct from the others. The T_m values of $[K(G5)_{1.5}]PF_6$ and $[K(G5)_2]PF_6$ are nearly equal to that of $[K(G5)_1]PF_6$, and these mixtures (and also more diluted systems) show thermal transitions due to G5 simultaneously.

Interestingly, the solid constituents precipitated from solution by storing certain diluted mixtures ($1 < n < 4$) for a few days at room temperature. These results imply a low affinity of $[K(G5)_1]PF_6$ for G5, and this is why the phase transitions of both $[K(G5)_1]PF_6$ and pure G5 appear in the binary mixtures involving excess G5. Additional phase transitions, other than the aforementioned thermal events, were also observed in the range of x = 0.25–0.55 (n = 3–0.8) at ca. −10 ºC. The largest peak was observed in the $[K(G5)_2]PF_6$ curve (**Figure S1**). Although the single phase has not been isolated, this result suggests the presence of a metastable 2:1 phase (n = 2) other than the equimolar complexes. The complicated peaks observed before melting for the mixtures are plotted in **Figure 1** as T_x.

Thermal properties: The T_m values of $[K(G5)_1]X$ are listed in **Table 1**. In comparison with the corresponding 18-crown-6 ether-K salt binary systems, all $[K(G5)_1]X$ equimolar mixtures possess relatively low T_m below 100 ºC (the T_m of $[K(18C6)_1][TFSA]$ is 162.9 ºC). Higher conformational flexibility of G5 compared to 18-crown-6 ethers causes a larger entropy change through melting, ΔS_m, and thus, T_m of the resulting complexes becomes lower ($T_m = \Delta H_m/\Delta S_m$, ΔH_m is the enthalpy of fusion). Interestingly, as well as typical ILs with onium cations,[64–66] the anionic structure strongly influences the T_m values of $[K(G5)_1]X$. It has been reported that the interionic interaction between parent cations and anions affects the T_m of glyme-Na complexes.[37] That interaction is closely related to the stabilization energy of ion pair formation, E_{form}, for parent salts. *Ab initio* quantum calculations were performed to yield the E_{form} of the studied parent K salts. The optimized structures of these salts are included in the Supporting Information (**Figure S2**). The calculated E_{form} values were −102.1, −105.6, −101.1, −103.6 and −103.8 kcal/mol for KPF_6, K[TfO], K[TFSA], KSCN, and K[NfO], respectively, indicating that the order of the calculated E_{form} is inconsistent with the T_m order: $[K(G5)_1]PF_6$ > $[K(G5)_1][TfO]$ > $[K(G5)_1][TFSA]$ > $[K(G5)_1]SCN$ > $[K(G5)_1][NfO]$. This result suggests the presence of other significant factors that determine T_m. The T_m values of typical imidazolium-based ILs are influenced not only by interionic interactions but also conformational flexibility of component ions and packing structures in the crystalline state.[67–69] Conformational flexibility due to long fluoroalkyl chains within the $[NfO]^-$ anion and multiple coordination structures caused by an SCN^- anion possibly lead to an

unexpectedly low T_m of $[K(G5)_1][NfO]$ and $[K(G5)_1]SCN$. On the other hand, the T_m value of $[K(G5)_1][TfO]$ was lower than $[K(G5)_1]PF_6$ even though the E_{form} of K[TfO] is larger than that of KPF_6. The cause of this phenomenon will be discussed in the next section.

Table 1. Melting points (T_m) and thermal decomposition temperature (T_d) for the studied $[K(G5)_1]X$ and pure G5.

Sample	T_m / ºC	T_d / ºC
Pure G5	−17.0	162
$[K(G5)_1][TFSA]$	35.9	220
$[K(G5)_1][TfO]$	39.6	177
$[K(G5)_1][NfO]$	8.6	190
$[K(G5)_1]PF_6$	47.9	176
$[K(G5)_1]SCN$	34.1	180

From the thermal stability measurements, we can judge whether the binary mixtures of G5 and K salts form stable complexes or not. The thermal stability of different composition of $[K(G5)_n]X$ was evaluated by TG, and the TG curves were included in the Supporting Information (**Figure S3**). Like the glyme-Li and glyme-Na salt systems,[19,37] the thermal stability of mixtures improves with increasing salt concentration. It should be noted that mass loss in these systems occurs by evaporation of uncoordinated (or highly exchangeable) glyme molecules. Interestingly, although DSC results suggest the presence of metastable phases, a corresponding stepwise mass change could not be observed in the TG curves of dilute mixtures containing excess glyme. These results strongly suggest exceptionally high thermal stability of $[K(G5)_1]^+$ complex cations.

Differences in the thermal decomposition temperature (ΔT_d) between $[K(G5)_1]X$ and pure G5 are shown in **Figure 2**. The thermal stability of $[K(G5)_1]X$ strongly depends on the paired anion species. $[K(G5)_1][TFSA]$ was stable up to 200 ºC (Table 1). $[K(G5)_1][NfO]$ was also relatively stable, whereas the ΔT_d values of the other equimolar complexes were lower. These results suggest that the interaction between K^+ cations and anions (K^+–X^-) affects the interaction between K^+ cations and glymes (K^+–

glyme). Because the K^+–X^- interaction screens the positive charge on K^+ cations, stronger K^+–X^- interactions leads to weaker ion dipole (K^+–glyme) interactions. As mentioned before, the E_{form} of the parent salts (K^+–X^- interaction) is in the order as follows: K[TfO] > K[NfO] > KSCN > KPF_6 > K[TFSA], suggesting that the weak K^+–$[TFSA]^-$ interaction causes high thermal stability in $[K(G5)_1][TFSA]$. We have no precise explanation for the relatively high T_d of $[K(G5)_1][NfO]$; however, the cohesive nature of the long fluoroalkyl groups of $[NfO]^-$ anions can impart strong K^+–glyme interactions.

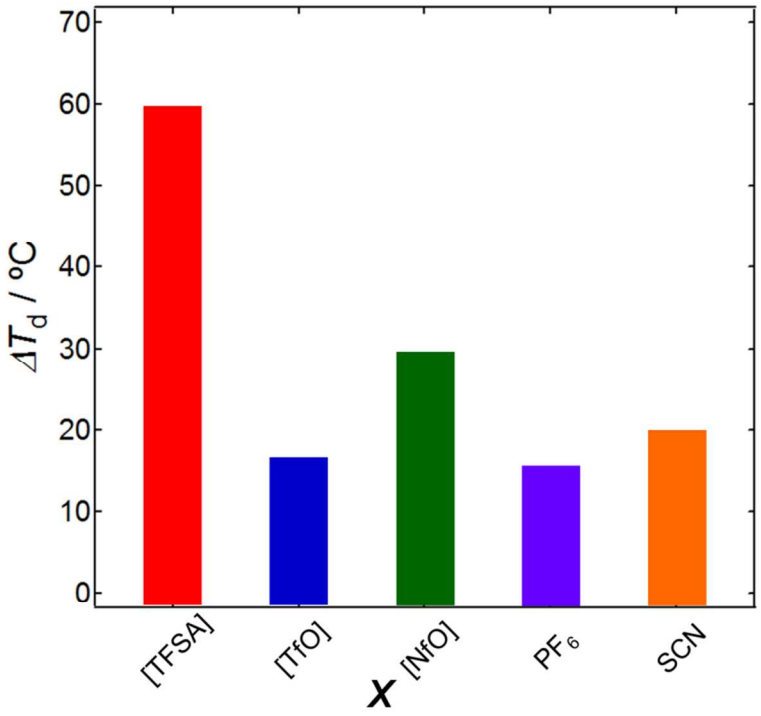

Figure 2. ΔT_d of $[K(G5)_1]X$ paired with $[TFSA]^-$, $[TfO]^-$, $[NfO]^-$, PF_6^-, and SCN^- anions.

3.2 Solvate structures in the crystalline state

Single-crystal structures of $[K(G5)_1][TFSA]$, $[K(G5)_1]PF_6$, and $[K(18C6)_1][TFSA]$ have been reported before.[23] In this study, the crystal structure of $[K(G5)_1][TfO]$ was clarified. The crystallographic data of $[K(G5)_1][TfO]$ is summarized in **Table S1**, and the thermal ellipsoid models of the solved structure are shown in the Supporting Information (**Figure S4**). Because of the low T_m and

low crystallinity, single crystals of $[K(G5)_1][NfO]$ and $[K(G5)_1]SCN$ could not be obtained. Instead, the single crystal structure of the corresponding crown-ether based complex, $[K(18C6)_1]SCN$, was successfully solved. The structures of $[K(18C6)_1][TfO]$, and $[K(18C6)_1]PF_6$ were also clarified. Their crystallographic data and solvate structures in the crystalline state were included in Supporting Information (**Table S1** and **Figures S5–S7**), and were employed to extrapolate the solvate structures of the glyme complexes more precisely.

Figure 3 illustrates the solvate structures of $[K(G5)_1][TFSA]$, $[K(G5)_1][TfO]$, and $[K(G5)_1]PF_6$ in the crystalline state along the *b*-axis. They form characteristic solvate structures. In the crystals, K^+ cations were typically coordinated by six oxygen atoms from a single G5 molecule and two oxygen ([TFSA] and [TfO]) or fluorine (PF_6) atoms from each anion, resulting in the octa-coordinated solvates. For the $[K(G5)_1][TFSA]$ solvate, nona-coordinated K^+ cation, where an additional fluorine atom from the trifluoromethyl group also coordinates to K^+ cation, was observed.[23] As shown in **Figure 3**, the coordination manner of anions was different depending on the complexes. One anion coordinates to two different K^+ cations in $[K(G5)_1][TFSA]$ and $[K(G5)_1]PF_6$, resulting in the aggregate type (AGG) solvates. On the other hand, for the $[K(G5)_1][TfO]$ solvate, two oxygen atoms of a single $[TfO]^-$ anion coordinate to a single K^+ cation in a bidentate form, leading to CIP-II (contact ion pair with a bidentate anion) type solvate. These differences were also seen in the corresponding crown-ether based complexes (ref. 23, **Figures S5 and S6**). As shown in **Figure S7**, $[K(18C6)_1]SCN$ belongs to the AGG type solvate, suggesting that $[K(G5)_1]SCN$ also forms an analogous structure in the crystalline state. Anionic structure dependence on the solvate structures has been reported for glyme-Li and glyme-Na equimolar complexes,[27,28,37] and this observation in $[K(G5)_1]X$ structures agrees well with that observed in $[Na(G4)_1][TFSA]$ (AGG) and $[Na(G4)_1]ClO_4$ (CIP-II). The cause of this phenomenon in $[Na(G4)_1]X$ complexes was closely related to the E_{form} of the parent salts: glyme-Na equimolar complexes with higher E_{form} tend to form CIP-II. The anionic effect on solvate types seen in $[K(G5)_1]X$ can be explained in a similar manner to the glyme-Na equimolar complexes. Furthermore, the lower T_m of $[K(G5)_1][TfO]$

compared to $[K(G5)_1]PF_6$ probably arises from this structural difference, CIP-II for the former and AGG for the latter.

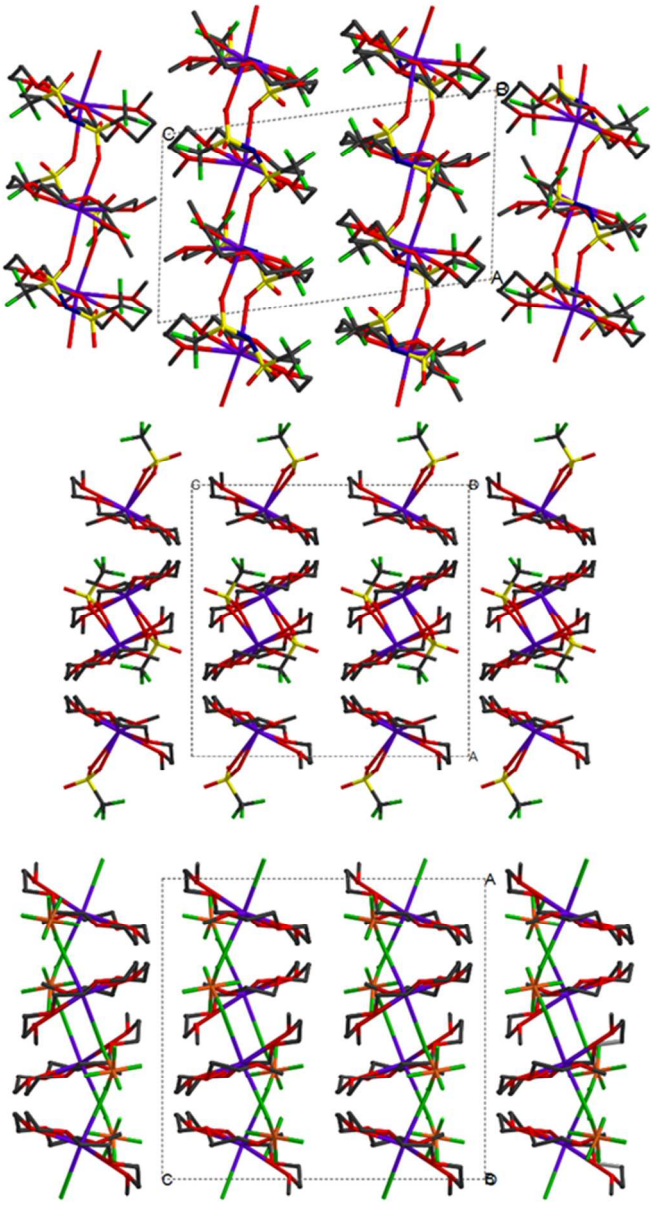

Figure 3. Packing diagrams of $[K(G5)_1][TFSA]$ (upper), $[K(G5)_1][TfO]$ (middle), and $[K(G5)_1]PF_6$ (lower) along the *b*-axis. Disorder atoms and H atoms are omitted for clarity. Purple K; red, O; gray, C; blue, N; yellow, S; green, F; orange, P.

Although the solvate types of $[K(G5)_1]X$ differ depending on the paired anionic structures, the coordination manner of the glymes to K^+ cations was similar. In these solvates, the glyme molecules coordinate to K^+ cations with a characteristic framework, as seen in 18-crown-6 ether-based complexes.

The conformations of the coordinating glymes are as follows: *tgt-tg't-tgt-tg't-tgt*, *tgt-tg't-tgt-tg't-tgt*, and *tg't-tgt-tg't-tgt-tg't* for $[K(G5)_1][TFSA]$, $[K(G5)_1][TfO]$, and $[K(G5)_1]PF_6$, respectively, where *t* and *g* mean *trans* and *gauche* conformations, respectively (**Table S2**). The distances between K^+ cation and oxygen atoms within glymes ($K–O_{glyme}$) were 2.826–2.913, 2.882–2.943, and 2.820–2.910 Å for $[K(G5)_1][TFSA]$, $[K(G5)_1][TfO]$, and $[K(G5)_1]PF_6$, respectively (**Table S3**). Stronger $K^+–X^-$ interaction of the parent K[TfO] salt should lead to weaker K^+–glyme interaction, resulting in relatively longer $K–O_{glyme}$ distances for $[K(G5)_1][TfO]$.

3.3 Raman spectra: concentration effect and solvate structure in the liquid state

Raman spectroscopy is one of the most powerful methods for evaluating complexation in glyme-salt mixtures. In the case of glyme-Li and glyme-Na systems, characteristic Raman bands were observed at ca. 870 cm^{-1}, the so-called breathing mode.[23,30,37,42] This band corresponds to the combination of COC stretching and CH_2 rocking modes of the coordinating ligand molecules, and is one of the fingerprint modes for the complex formation. Conveniently, certain anionic Raman bands are sensitive to the variation of the coordination manner of the anions. In this section, we discuss the effect of concentration on the coordination environment around K^+ cations based on the spectral variation of the representative cationic and anionic Raman bands. From the temperature dependent spectra, the solvate structures in the (molten) liquid state are also examined.

Concentration effect: Cationic Raman spectra of $[K(G5)_n]X$ at different concentrations are shown in **Figure 4**. Spectral correction was carried out by using the salt concentration and the peak areas of the representative anionic bands. This figure clearly illustrates that the intensity of the broad Raman bands observed around 850 cm^{-1}, attributable to free G5, decreased as the K salt concentration increased, while the representative peak at ca. 870 cm^{-1} emerged simultaneously, irrespective of the paired anion species. This result suggests that the formation of the $[K(G5)_1]^+$ complex cation proceeds even at low concentrations by consuming free glymes with the addition of K salts. At the 1:1 composition, except for $[K(G5)_1][NfO]$, the bands attributable to the uncoordinated free glyme completely vanished,

implying that the binary mixtures of G5 and K salts formed complexes in a 1:1 relationship. These observations agree well with the phase diagrams (**Figure 1**). Although the Raman spectra of $[K(G5)_n][NfO]$ indicates the formation of certain complexes, broad bands still remained even at equimolar composition, suggesting the presence of some free glymes.

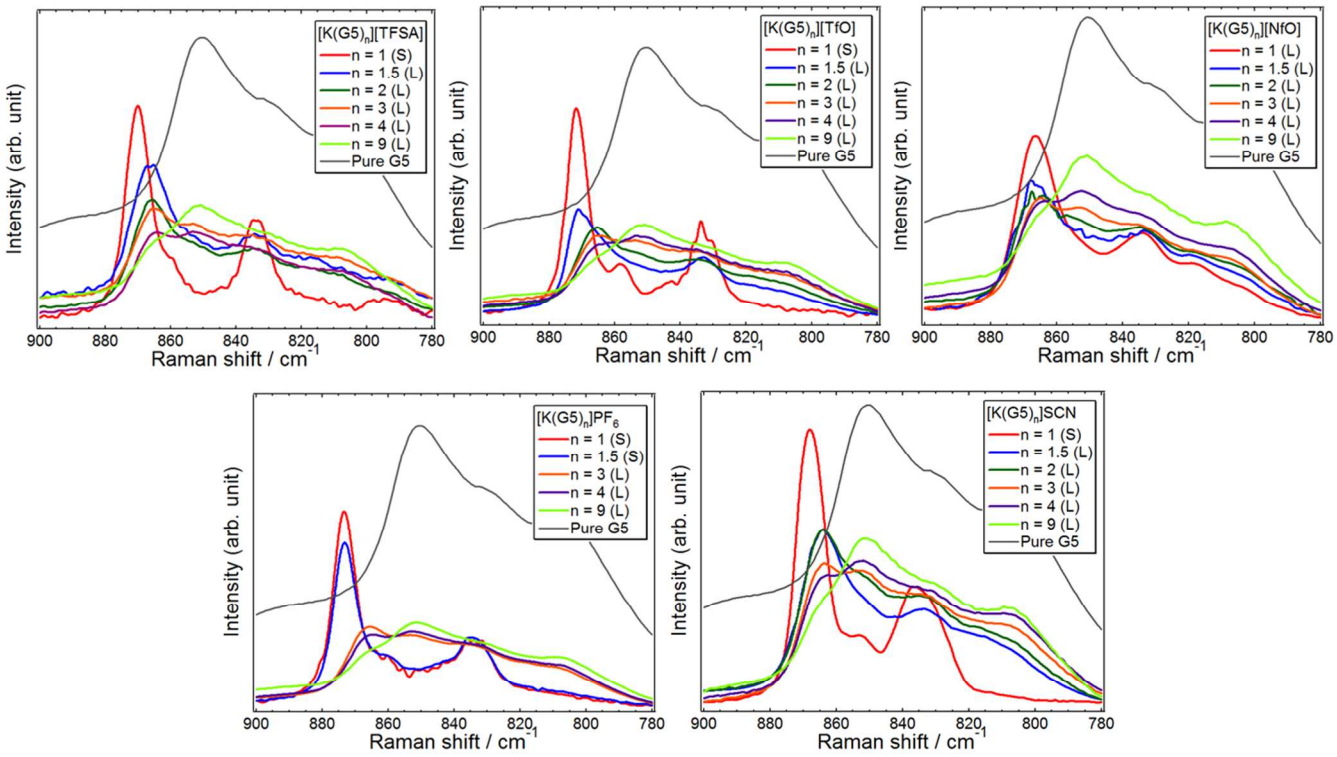

Figure 4. Concentration dependence of cationic Raman spectra for G5-KX mixtures paired with $[TFSA]^-$, $[TfO]^-$, $[NfO]^-$, PF_6^-, and SCN^- anions. The Raman spectrum of pure G5 was also included in each figure. The captions of "S" and "L" in each legend mean "solid" and "liquid" states, respectively.

Taking into account the concentration dependence of the Raman spectra of G5-KPF_6 systems, the spectral shapes of $[K(G5)_1]PF_6$ and $[K(G5)_{1.5}]PF_6$ seem similar as both samples are in the solid state. As described in the previous section, phase separation (precipitation) occurs in $[K(G5)_{1.5}]PF_6$ and $[K(G5)_2]PF_6$ by storing them for a few days. Separating the supernatant liquid from the precipitated solid of $[K(G5)_2]PF_6$, and then measuring their Raman spectra showed that the liquid and solid constituents were similar to those of pure G5 and $[K(G5)_1]PF_6$, respectively (**Figure S8**).

Variation in the anionic Raman spectra provides useful information on the coordination manner of the anions and the dissociation state of the parent salts. The concentration dependence of the anionic spectra for $[K(G5)_n]X$ with different anions are shown in **Figure 5**. Each spectral range adopted in this study corresponds to the anionic vibrational modes as follows: expansion-contraction modes for the entire $[TFSA]^-$, S–O stretching modes for $[TfO]^-$ and $[NfO]^-$, P–F stretching modes for PF_6^-, and C–S stretching modes for SCN^- anions. The anion dependent spectral variation can be observed. For G5-KX mixtures with $[TFSA]^-$, $[NfO]^-$, and PF_6^- anions, the spectral shapes and frequencies for each anion were similar irrespective of the salt concentration. For G5-K[TfO] mixtures, the S–O stretching mode would slightly shift to the low-frequency side as the salt concentration increased. In the case of Li[TfO], the reported S–O stretching modes observed at 1032, 1042, and 1052 cm^{-1} are assigned to free (uncoordinated) ions, CIP, and AGG, respectively.[45–47] Based on the crystal structure of $[K(G5)_1][TfO]$, the $[TfO]^-$ anions in this crystalline equimolar complex coordinate to K^+ cations in a bidentate form, resulting in CIP-II type solvate (**Figure 3**). Thus, the concentration dependent shift of $[TfO]^-$ anions to the low-frequency side observed in G5-K[TfO] mixtures could be attributed to the variation of AGG to CIP. The pronounced anionic spectral variation was observed for G5-KSCN mixtures. In dilute systems ($n > 1$), two peaks at ca. 745 and 733 cm^{-1} were observed. At the equimolar composition, a single peak appeared at 745 cm^{-1}, suggesting that the coordination manner of the SCN^- anions is concentration dependent. Evtushenko et al. assigned the bands at 745 and 733 cm^{-1} to free SCN^- anions and K–SCN coordination, respectively.[51] Although there is no information on the coordination manner of SCN^- anion in $[K(G5)_1]SCN$, the single crystal structure of $[K(18C6)_1]SCN$ was clarified. In this complex, both K–SCN and K–NCS forms can be seen in the crystalline state (see **Figure S7**). In the Raman spectrum of $[K(18C6)_1]SCN$ crystal (**Figure S9**), a single peak appears at 735 cm^{-1}, corresponding to the modes of SCN^- anions participating in coordination to K^+ cations. From this spectrum, it can be speculated that SCN^- anions do not participate in coordination to K^+ cations in $[K(G5)_1]SCN$ crystals thereby forming a solvent-separated ion pair type solvate, even though the coordinating SCN^- anions are present in dilute mixtures ($n > 1$).

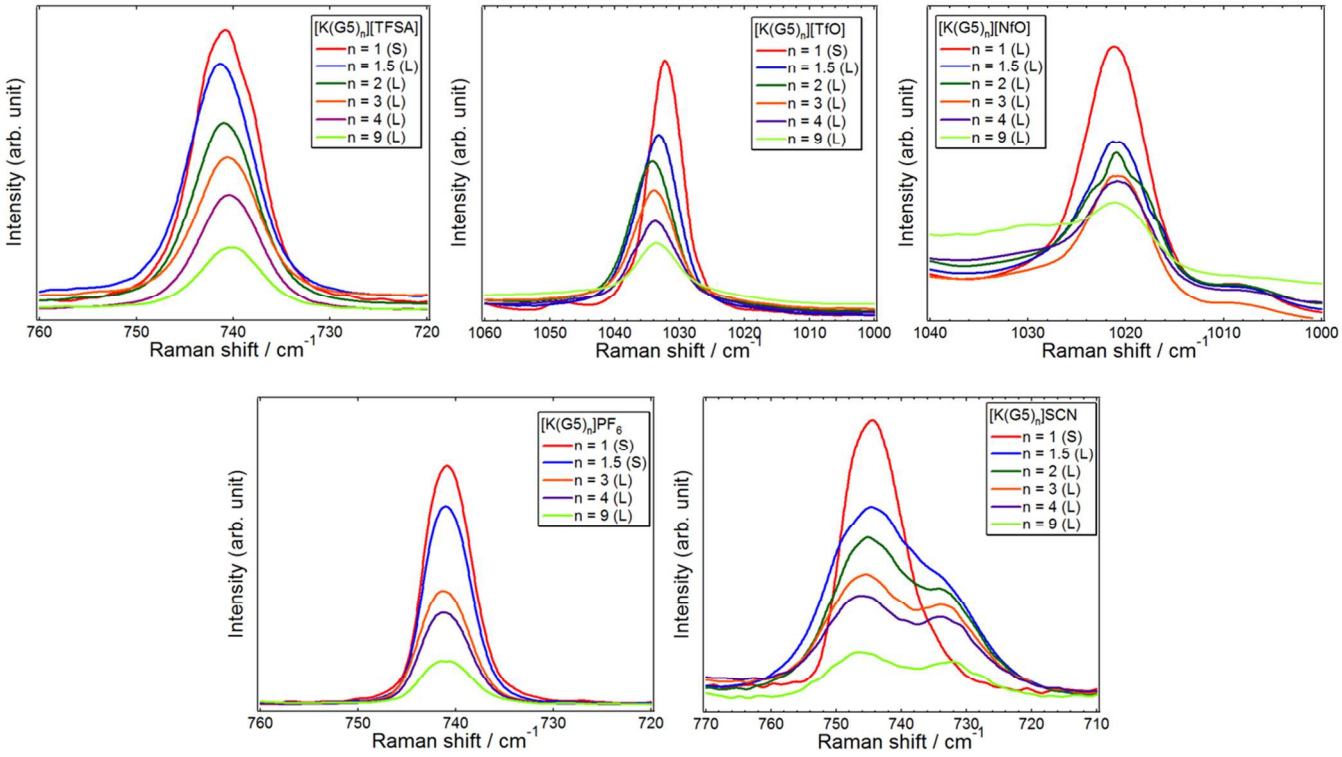

Figure 5. Concentration dependence of anionic Raman spectra for G5-KX mixtures paired with $[TFSA]^-$, $[TfO]^-$, $[NfO]^-$, PF_6^-, and SCN^- anions. The captions "S" and "L" in each legend mean "solid" and "liquid" states, respectively.

Equimolar complexes and their structures in the liquid state: The frequencies of the representative Raman bands observed in the cationic and anionic spectra for 1:1 complexes are summarized in **Table 2**. In addition, anionic Raman spectra and representative Raman frequencies for the corresponding crown-ether based complexes are also included in the Supporting Information (**Figure S9** and **Table S4**). The cationic spectra have bands at nearly identical frequency, ca. 870 and 835 cm^{-1}, irrespective of the paired anion species. In the case of $[Li(glyme)_n]X$ and $[Na(glyme)_1]X$, the cationic spectra varied depending on the solvate structure of the complexes.[30,37] Therefore, these results indicate that the coordination manner of glymes in $[K(G5)_1]X$ with different anions was nearly identical, which supports our speculation on the unsolved solvate structures of the $[K(G5)_1][NfO]$ and $[K(G5)_1]SCN$ complexes.

Table 2. Selected vibrational frequencies of the coordinating glymes and counter anions observed in the Raman spectra of $[K(G5)_1]X$.

	Raman shift / cm^{-1}				
	$[K(G5)_1][TFSA]$	$[K(G5)_1][TfO]$	$[K(G5)_1][NfO]$	$[K(G5)_1]PF_6$	$[K(G5)_1]SCN$
Coordinating glyme	870	872	866	873	868
	835	834	834	832	837
Counter anions	741	1032	1021	741	745

The anionic spectrum of $[K(G5)_1][NfO]$ in the liquid state was similar to that of $[K(18C6)_1][NfO]$ in the crystalline state, as shown in **Figures 5** and **S9**. In the case of the complexes paired with the structurally analogous $[TfO]^-$ anion, both $[K(G5)_1][TfO]$ and $[K(18C6)_1][TfO]$ form CIP-II type solvate, and they showed similar anionic spectra in the crystalline state. These results suggest that $[NfO]^-$ anions in molten $[K(G5)_1][NfO]$ coordinate to K^+ cations in a similar manner to those in crystalline $[K(18C6)_1][NfO]$.

As described above, although the solvate structures of the equimolar complexes in the crystalline state were clarified by X-ray crystallography, there was no information on the structures in the liquid state. The solvate structures in the liquid state are important because they are closely related to the ionic nature and the properties of the molten complexes, especially their ionic conductivity. By considering the Raman spectra of both the crystalline and liquid states, the solvate structures of $[K(G5)_1]X$ in the liquid state were elucidated.

Each sample was enclosed in a capillary and the Raman spectra were collected at different temperatures (20, 50, and 80 ºC). $[K(G5)_1][NfO]$ was in the liquid state at all applied temperatures. Temperature dependent Raman spectra in the range of 900–700 cm^{-1} are illustrated in **Figure 6**. The cationic spectral shape of $[K(G5)_1][TFSA]$ and $[K(G5)_1]PF_6$ was insensitive to the phase state and temperature, suggesting that glymes coordinate to K^+ cations in a similar manner in both liquid and crystalline states. In the case of $[K(G5)_1]SCN$, the breathing modes still appeared in the liquid state,

however, broad bands attributable to free glymes were also observed at 850–780 cm^{-1} as the temperature increased. In addition, the band due to the C–S stretching mode of the SCN^- anion at ca. 745 cm^{-1} was broadened. This result strongly suggests that the solvate structures in the crystalline state were partially broken by melting, resulting in the release of free glymes. In particular, the spectral shape of $[K(G5)_1][TfO]$ varied considerably upon melting. The sharp peak observed at ca. 755 cm^{-1} in the crystalline state was assigned to the C–F stretching mode of $[TfO]^-$ anion, and this peak was also sensitive to the variation of coordination environment of the anion.[45] In the liquid state, the spectral shape, especially the representative bands due to the complex cation (ca. 870 and 835 cm^{-1}) and $[TfO]^-$ anion (755 cm^{-1}), varied considerably. The representative cationic bands shifted to the low-frequency side and the anionic band splits into two sharp peaks. The cationic spectral shape at 80 ºC was similar to that of free glyme, suggesting that a large amount of free (or highly exchangeable) glymes emerged by breaking the solvate structure. The anionic spectral variation also supports the change in the solvate structure of $[K(G5)_1][TfO]$ upon melting.

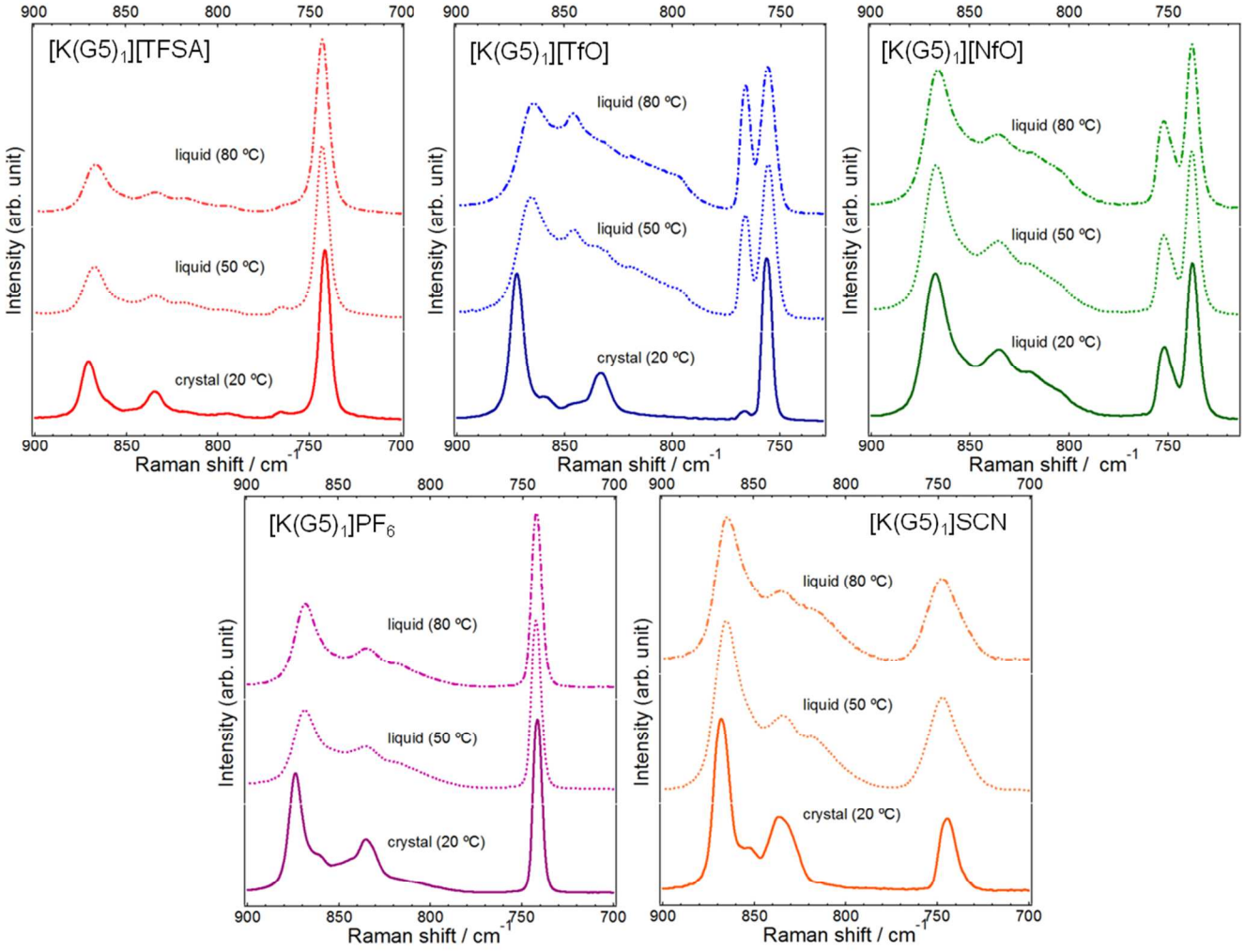

Figure 6. The effect of temperature on the Raman spectra of $[K(G5)_1][X]$ with $[TFSA]^-$, $[TfO]^-$, $[NfO]^-$, PF_6^-, and SCN^- anions.

Except for $[K(G5)_1][NfO]$, the degree of spectral variation by melting depended strongly on the paired anion species, in the order as follows: $[TfO]^- > SCN^- > PF_6^- \geq [TFSA]^-$. This order is completely consistent with that of the E_{form} of the parent salts. Therefore, it can be concluded that the solvate stability is closely related to the ion-ion interaction of the parent salts, and stable complexes can be achieved only when the G5–K^+ interaction overwhelms ion–ion interactions, such as the system paired with the weak Lewis basic $[TFSA]^-$ anion. These phenomena have also been reported for glyme-Li systems; the Lewis basicity of the paired anion species has a strong impact on the solvate stability of the equimolar complexes.[21]

3.4 Physicochemical properties

Table 3 summarizes the physicochemical properties, such as density (ρ), concentration (c), viscosity (η), and ionic conductivity (σ), determined in this study for $[K(G5)_1][TFSA]$, $[K(G5)_1][NfO]$, and $[K(G5)_1]SCN$ at 40 ºC. The relatively high crystallinity of $[K(G5)_1][TfO]$ and $[K(G5)_1]PF_6$ made it difficult to measure the properties of these complexes. By considering all the various properties and structural aspects, the ionic nature of $[K(G5)_1]X$ was elucidated.

Table 3. Transport properties for $[K(G5)_1][TFSA]$, $[K(G5)_1][NfO]$, and $[K(G5)_1]SCN$ at 40 ºC.

	F. W. / g mol^{-1}	ρ / g cm^{-3}	c / mol dm^{-3}	η / mPa s	σ / mS cm^{-1}	$\Lambda_{imp}/\Lambda_{ideal}$
$[K(G5)_1][TFSA]$	585.58	1.384	2.364	115.7	1.14	0.56
$[K(G5)_1][NfO]$	604.52	1.407	2.327	131.7	0.52	0.30
$[K(G5)_1]SCN$	363.51	1.170	3.218	178.1	0.93	0.51

Liquid density and concentration: The temperature dependence of ρ was evaluated in the temperature range of 40–80 ºC. The c values of the equimolar mixtures were calculated by using the ρ and formula weight. These results are included in the Supporting Information (**Figure S10**). As shown in **Figure S10**, ρ decreased as the temperature increased, and the order of ρ for the mixtures with different anionic structures at the same temperature is as follows: $[K(G5)_1][NfO] > [K(G5)_1][TFSA] > [K(G5)_1]SCN$ (**Table 3**). A large number of fluorine atoms within a single anion caused high ρ in $[K(G5)_1][TFSA]$ and $[K(G5)_1][NfO]$. The c values for the mixtures at the same temperature showed inverse order to ρ. $[K(G5)_1]SCN$ has an exceptionally high c (3.2 mol dm^{-3}) compared to the others (ca. 2.3 mol dm^{-3}), as a result of the low formula weight of the parent KSCN salt and the molar volume of SCN^- anions.

Viscosity and ionic conductivity: The temperature dependences of η and σ for $[K(G5)_1][TFSA]$, $[K(G5)_1][NfO]$, and $[K(G5)_1]SCN$ are displayed in **Figure S11**. Both parameters exhibit non-Arrhenius

type temperature dependent behavior. As listed in **Table 3**, the η values at 40 ºC were 115.7, 131.7, 178.1 mPa·s for $[K(G5)_1][TFSA]$, $[K(G5)_1][NfO]$, and $[K(G5)_1]SCN$, respectively. Strong interionic interactions per unit volume, due to high c, probably leads to high η in $[K(G5)_1]SCN$. On the other hand, η of $[K(G5)_1][NfO]$ was higher than that of $[K(G5)_1][TFSA]$ despite both having comparable c. This phenomenon probably arises from a strong cation–anion interaction (E_{form}) and the flexibility of the perfluorobutyl group within a $[NfO]^-$ anion.[70] Interestingly, taking notice of σ, the values for $[K(G5)_1][NfO]$ were considerably lower than those for $[K(G5)_1][TFSA]$ and $[K(G5)_1]SCN$. Because σ is a function of the number and mobility of charge carriers, c and η are the predominant factors that affect σ. However, the low σ observed in $[K(G5)_1][NfO]$ cannot be explained in terms of only these parameters, and hence, this result suggests the existence of other significant factors. For typical ILs, because they can be regarded as extremely concentrated electrolytes, the dissociativity or correlation of ionic motion resulting from interplay between anions and cations (i.e., ionicity) strongly affects their ionic nature. The c values listed in **Table 3** do not correspond to the net "ionic concentration". Therefore, the dissociativity of the mixtures was evaluated by means of Walden's rule, and their ionic nature will be discussed.

Anionic and cationic effect on ionic nature: The Walden plots for $[K(G5)_1][TFSA]$, $[K(G5)_1][NfO]$, and $[K(G5)_1]SCN$ are depicted in **Figure 9**. In this figure, Λ_{imp} means the molar conductivity defined as σ/c. The ideal KCl aqueous solution where K^+ cations and Cl^- anions are completely dissociated is considered to afford an ideal straight line with a slope of unity in Walden plots. This figure clearly illustrates that while the plots of $[K(G5)_1][TFSA]$ and $[K(G5)_1]SCN$ are located near the ideal line, $[K(G5)_1][NfO]$ deviated from the ideal appreciably, suggesting high associativity between K^+ and $[NfO]^-$. The dissociativity can be estimated roughly by the ionicity defined as $\Lambda_{imp}/\Lambda_{ideal}$, where Λ_{ideal} denotes the ideal molar conductivity based on the ideal line. These values at 40 ºC are also included in **Table 3**. The ionicity of $[K(G5)_1][NfO]$ was lower than the others. Angell et al. classified protic ILs into four groups by means of the deviation of the Walden plots from the ideal line (namely ionicity): super ILs (exceeds the ideal line), good ILs (near the ideal), poor ILs (moderately deviated from the ideal),

and non-ILs (far from the ideal).[71] In a recent article, we also proposed subdivision of solvate ILs into "good" and "poor", based on their chemical nature.[24] On the basis of these classifications, $[K(G5)_1][NfO]$ should belong to poor solvate ILs, indicating that K^+ cations and $[NfO]^-$ anions are mutually associated and present as neutral species rather than the cases of $[K(G5)_1][TFSA]$ and $[K(G5)_1]SCN$. On the other hand, the ionicity of $[K(G5)_1]SCN$ is similar to that of $[K(G5)_1][TFSA]$ although the Raman results imply destruction of solvate structure by melting, suggesting that K^+ and SCN^- ions are still dissociated even in the liquid state. $[K(G5)_1][TFSA]$ shows the highest ionicity of the three mixtures, and this value is nearly consistent with the representative solvate IL, $[Li(glyme)_1][TFSA]$.[19] Therefore, $[K(G5)_1][TFSA]$ can be classified as a "good" solvate IL. On the basis of their chemical nature, $[K(G5)_1]X$ complexes paired with $[TfO]^-$, $[NfO]^-$, PF_6^-, and SCN^- anions are considered to be "poor" solvate ILs.

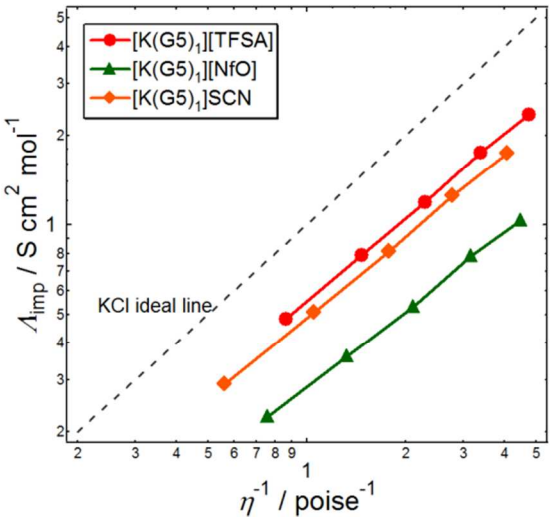

Figure 9. Walden plots for $[K(G5)_1][TFSA]$, $[K(G5)_1][NfO]$, and $[K(G5)_1]SCN$ with KCl ideal line.

Previously, we reported that $[Li(glyme)_1]ClO_4$ showed solvate IL features.[21] Moreover, equimolar mixing of $NaClO_4$ and certain glymes (G4 or G5) also provides relatively stable complexes.[37] However, $KClO_4$ is hardly soluble in G5, implying that cationic species (Lewis acidity) is also a predominant factor affecting the ionic nature of the mixtures. The increase in cationic size decreases the interactions

of cations with glymes and anions. Owing to the large contribution of the induction interaction (induced polarization) to the attraction between the cation and glyme, the cationic size affects the susceptibly of the cation–glyme interaction rather than the cation–anion interaction. Moreover, the induced polarization decreases rapidly with distance, while the electrostatic interaction between cation and anion decreases gradually.[72] As a result, the increase in the cationic size enhances the relative stability of the cation–anion complexes compared with that of the cation–glyme complexes. This is why the limited equimolar complex, incorporating parent K salt with rather weak ion–ion interaction, can be classified as good solvate ILs. Therefore, it can be concluded that an appropriate combination of anionic structures and cationic metal species is critical for realizing "good" solvate ILs which behave similarly to typical aprotic ILs in the molten state.

4. CONCLUSIONS

The phase behavior, solvate structures, and physicochemical properties of a series of glyme-K salt binary mixtures, $[K(G5)_n]X$, were explored. The T_m values exhibited maxima at the equimolar composition irrespective of the paired anion species. The thermal stability of equimolar mixtures, $[K(G5)_1]X$, depended strongly on the paired anionic structure, and $[K(G5)_1][TFSA]$ was stable up to 200 ºC. X-ray crystallography revealed that G5 molecules coordinate to K^+ cations in a characteristic manner like 18-crown-6 ether does. These results clearly showed that $[K(G5)_1]^+$ complexes form in the equimolar binary mixtures. Raman spectra of the different states suggest that the stability of the studied complexes strongly depends on the ion–ion interaction (E_{form}) of the parent salts. Characteristic spectral variation was observed in the temperature dependent $[K(G5)_1][TfO]$ spectra, indicating that the solvate structure in the crystalline state would be broken by phase transition. These results agree with the anionic structure dependence of the thermal stability for the equimolar mixtures. Furthermore, the Walden plots of certain liquid samples clearly reflects their ionic nature. Judging from the dissociativity (ionicity) and the solvation environment in the liquid state, $[K(G5)_1][TFSA]$ possesses enough potential

regarding as ILs, thus can be classified as a solvate IL. According to studies of the glyme-alkali metal salt binary mixtures, anionic Lewis basicity and cationic Lewis acidity have a strong impact on whether they belong to (good) solvate ILs or not.

ACKNOWLEDGMENT: This study was supported in part by the Advanced Low Carbon Technology Research and Development Program (ALCA) of the Japan Science and Technology Agency (JST), the Technology Research Grant Program of the New Energy and Industrial Technology Development Organization (NEDO) of Japan, and MEXT program "Elements Strategy Initiative to Form Core Research Center", Ministry of Education Culture, Sports, Science and Technology (MEXT) of Japan.

REFERENCES

1. J. Tang, H. Tang, W. Sun, H. Plancher, M. Radosz, Y. Shen, *Chem. Commun*., 2005, 3325–3327.
2. A. Roche, T. Carvalho, P. Vidinha, N. M. T. Lourenço, *ChemPlusChem*, 2012, 77, 1106–1111.
3. H. Zhao, O. Olubajo, Z. Song, A. L. Sims, T. E. Person, R. A. Lawal, L. A. Holley, *Bioorg. Chem*., 2006, **34**, 15–25.
4. K. Fujita, D. R. MacFarlane, M. Forsyth, Y.-M. Fujita, K. Murata, N. Nakamura, H. Ohno, *Biomacromolecules*, 2007, **8**, 2080–2086.
5. A. P. Abbott, J. C. Barron, K. S. Ryder, D. Wilson, *Chem. Eur. J*., 2007, **13**, 6495–6501.
6. Q. Zhang, K. D. O. Vigier, S. Royer, F. Jérôme, F. *Chem. Soc. Rev*., 2012, **41**, 7108–7146.
7. T. Tsuda, K. Kondo, M. Baba, S. Suwa, Y. Ikeda, T. Sakamoto, S. Seino, H. Yoshida, M. Ozaki, A. Imanishi, S. Kuwabata, *Electrochim. Acta*, 2013, **100**, 285–292.
8. T. Tamura, K. Yoshida, T. Hachida, M. Tsuchiya, M. Nakamura, Y. Kazue, N. Tachikawa, K. Dokko, M. Watanabe, *Chem. Lett.*, 2010, **39**, 753–755.
9. K. Yoshida, M. Nakamura, Y. Kazue, N. Tachikawa, S. Tsuzuki, S. Seki, K. Dokko, M. Watanabe, *J. Am. Chem. Soc.*, 2011, **133**, 13121–13129.
10. K. Yoshida, M. Tsuchiya, N. Tachikawa, K. Dokko, M. Watanabe, *J. Electrochem. Soc*., 2012, **159**, A1005–A1012.
11. S. Seki, K. Takei, H. Miyashiro, M. Watanabe, *J. Electrochem. Soc.*, 2011, **158**, A769-A774.
12. K. Dokko, N. Tachikawa, K. Yamauchi, M. Tsuchiya, A. Yamazaki, E. Takashima, J.-W. Park, K. Ueno, S. Seki, N. Serizawa, M. Watanabe, *J. Electrochem. Soc*., 2013, **160**, A1304–A1310.
13. K. Ueno, J.-W. Park, A. Yamazaki, T. Mandai, N. Tachikawa, K. Dokko, M. Watanabe, *J. Phys. Chem. C*, 2013, **117**, 20509–20516.
14. T. Inagaki, T. Mochida, *Chem. Lett.*, 2010, **39**, 572–573.
15. R. Hagiwara, T. Hirashige, T. Tsuda, Y. Ito, *J. Fluorine Chem.*, 1999, **99**, 1–3.
16. K. Matsumoto, T. Tsuda, R. Hagiwara, Y. Ito, O. Tamada, *Solid State Sci.*, 2002, **4**, 23–26.
17. K. M. Johansson, E. I. Izgorodina, M. Forsyth, D. R. MacFarlane, K. R. Seddon, *Phys. Chem.*

Chem. Phys., 2008, **10**, 2972–2978.

18. C. A. Angell, Y. Ansari, Z. Zhao, *Faraday Discussions*, 2012, **154**, 9–27.

19. K. Yoshida, M. Tsuchiya, N. Tachikawa, K. Dokko, M. Watanabe, *J. Phys, Chem. C*., 2011, **115**, 18384–18394.

20. T. M. Pappenfus, W. A. Henderson, B. B. Owens, K. R. Mann, W. H. Smyrl, *J. Electrochem. Soc*., 2004, **151**, A209–A215.

21. K. Ueno, K. Yoshida, M. Tsuchiya, N. Tachikawa, K. Dokko, M. Watanabe, *J. Phys. Chem. B*, 2012, **116**, 11323–11331.

22. C. Zhang, K. Ueno, A. Yamazaki, K. Yoshida, T. Mandai, Y. Umebayashi, K. Dokko, M. Watanabe, *J. Phys. Chem. B*, 2014, **118**, 5144–5153.

23. T. Mandai, K. Yoshida, S. Tsuzuki, R. Nozawa, H. Masu, K. Ueno, K. Dokko, M. Watanabe, *J. Phys, Chem. B*, 2014, *submitted.*

24. T. Mandai, K. Yoshida, K. Ueno, K. Dokko, M. Watanabe, *Phys. Chem. Chem. Phys*., 2014, **16**, 8761–8772.

25. Y. Choquette, G. Brisard, M. Parent, D. Brouillette, G. Perron, J. E. Desnoyers, M. Armand, D. Gravel, N. Slougi, *J. Electrochem. Soc*., 1998, **145**, 3500–3507.

26. W. A. Henderson, F. McKenna, M. A. Khan, N. R. Brooks, V. G. Young, Jr., R. Frech, *Chem. Mater.*, 2005, **17**, 2284–2289.

27. W. A. Henderson, N. R. Brooks, W. W. Brennessel, V. G. Young, Jr., *Chem. Mater*., 2003, **15**, 4679–4684.

28. W. A. Henderson, N. R. Brooks, V. G. Young, Jr., *Chem. Mater*., 2003, **15**, 4685–4690.

29. W. A. Henderson, *J. Phys. Chem. B*, 2006, **110**, 13177–13183.

30. D. Brouillette, D. E. Irish, N. J. Taylor, G. Perron, M. Odziemkowski, J. E. Desnoyers, *Phys. Chem. Chem. Phys.*, 2002, **4**, 6063–6071.

31. P. Johansson, J. Tegenfeldt, J. Lindgren, *Polymer*, 1999, **40**, 4399–4406.

32. N. R. Dhumal, S. P. Gejji, *J. Phys. Chem. A*, 2006, **110**, 219–227.

33. C. Zhang, D. Ainsworth, Y. G. Andreev, P. G. Bruce, *J. Am. Chem. Soc*., 2007, **129**, 8700–8701.

34. C. Zhang, S. J. Lilly, D. Ainsworth, E. Staunton, Y. G. Andreev, A. M. Z. Slawin, P. G. Bruce, *Chem. Mater*., 2008, **20**, 4039–4044.

35. N. Tachikawa, K. Yamauchi, E. Takashima, J.-W. Park, K. Dokko, M. Watanabe, *Chem. Commun*., 2011, **47**, 8157–8159.

36. R. Tatara, N. Tachikawa, H.-M. Kwon, K. Ueno, K. Dokko, M. Watanabe, *Chem. Lett*., 2013, **42**, 1053–1055.

37. T. Mandai, R. Nozawa, S. Tsuzuki, K. Yoshida, K. Ueno, K. Dokko, M. Watanabe, *J. Phys. Chem. B*, 2013, **117**, 15072–15085.

38. C. J. Pederson, *J. Am. Chem. Soc*., 1967, **88**, 7017–7036.

39. W. P. Fehlhammer, S. Schrolkamp, M. Hoyer, H. Hartl, W. Beck, *Z. Anorg. Allg. Chem*., 2005, **631**, 3025–3029.

40. V. L. Rudzevich, H. Gornitzka, K. Miqueu, J.-M. Sotiropoulos, G. P. Guillouzo, V. D. Romanenko, G. Bertrand, *Angew. Chem., Int. Ed*., 2002, **41**, 1193–1195.

41. R. E. A. Dillon, D. F. Shriver, *Solid State Ionics*, 2000, **132**, 93–99.

42. J. Grondin, J.-L. Lassègues, M. Chami, L. Servant, D. Talaga, W. A. Henderson, *Phys. Chem. Chem. Phys*., 2004, **6**, 4260–4267.

43. M. Herstedt, M. Smirnov, P. Johansson, M. Chami, J. Grondin, L. Servant, J. C. Lasségues, *J. Raman Spectrosc*., 2005, **36**, 762–770.

44. Y. Umebayashi, T. Mitsugi, S. Fukuda, T. Fujimori, K. Fujii, R. Kanzaki, M. Takeuchi, S. Ishiguro, *J. Phys. Chem. B*, 2007, **111**, 13028–13032.

45. W. Huang, R. Frech, R. A. Wheeler, *J. Phys. Chem*., 1994, **98**, 100–110.

46. J. M. Alía, H. G. M. Edwards, *Vib. Spectrosc*., 2000, **24**, 185–200.

47. F. Alloin, G. Hirankumar, T. Pagnier, *J. Phys. Chem. B*, 2009, **113**, 16465–16471.

48. E. R. Talaty, S. Raja, V. J. Storhaug, A. Dölle, W. R. Carper, *J. Phys. Chem. B*, 2004, **108**, 13177–13184.

49. C. M. Burba, R. Frech, *J. Phys. Chem. B*, 2005, **109**, 15161–15164.

50. J.-Y. Chien, *J. Am. Chem. Soc.*, 1947, **69**, 20–22.

51. N. P. Evtushenko, V. A. Sushko, S. V. Volkov, *Teoreticheskaya i Éksperimental'naya Khimiya*, 1973, **9**, 533–537.

52. A. Altomare, G. Cascarano, C. Giacovazzo, A. Guagliardi, M. C. Burla, G. Polidori, M. Camalli, *J. Appl. Cryst*., 1994, **27**, 435.

53. G. M. Sheldrick, *Program for the Refinement of Crystal Structures*, SHELX97. University of Göttingen, Germany, **1997**.

54. A short history of SHELX: G. M. Sheldrick, *Acta Crystallogr*., 2008, **A64**, 112−122.

55. CrystalStructure 4.0: Crystal Structure Analysis Package. Rigaku Corporation, Tokyo 196-8666, Japan, 2000–2010.

56. M. J. Frisch, G. W. Trucks, H. B. Schlegel, G. E. Scuseria, M. A. Robb, J. R. Cheeseman, J. A. Montgomery, Jr., T. Vreven, K. N. Kudin, J. C. Burant, J. M. Millam, S. S. Iyengar, J. Tomasi, V. Barone, B. Mennucci, M. Cossi, G. Scalmani, N. Rega, G. A. Petersson, H. Nakatsuji, M. Hada, M. Ehara, K. Toyota, R. Fukuda, J. Hasegawa, M. Ishida, T. Nakajima, Y. Honda, O. Kitao, H. Nakai, M. Klene, X. Li, J. E. Knox, H. P. Hratchian, J. B. Cross, V. Bakken, C. Adamo, J. Jaramillo, R. Gomperts, R. E. Stratmann, O. Yazyev, A. J. Austin, R. Cammi, C. Pomelli, J. W. Ochterski, P. Y. Ayala, K. Morokuma, G. A. Voth, P. Salvador, J. J. Dannenberg, V. G. Zakrzewski, S. Dapprich, A. D. Daniels, M. C. Strain, O. Farkas, D. K. Malick, A. D. Rabuck, K. Raghavachari, J. B. Foresman, J. V. Ortiz, Q. Cui, A. G. Baboul, S. Clifford, J. Cioslowski, B. B. Stefanov, G. Liu, A. Liashenko, P. Piskorz, I. Komaromi, R. L. Martin, D. J. Fox, T. Keith, M. A. Al-Laham, C. Y. Peng, A. Nanayakkara, M. Challacombe, P. M. W. Gill, B. Johnson, W. Chen, M. W. Wong, C. Gonzalez, J. A. Pople, GAUSSIAN 03 (Revision E.01), Gaussian, Inc., Wallingford, CT, 2004.

57. C. Mϕller, M. S. Plesset, *Phys. Rev.*, 1934, **46**, 618–622.

58. M. Head-Gordon, J. A. Pople, M. J. Frisch, *Chem. Phys. Lett*., 1988, ***153***, 503–506.

59. B. J. Ransil, *J. Chem. Phys*., 1961, **34**, 2109–2118.

60. S. F. Boys. F. Bernardi, *Mol. Phys*., 1970, **19**, 553–556.

61. S. Tsuzuki, H. Tokuda, K. Hayamizu, M. Watanabe, *J. Phys. Chem. B*, 2005, **109**, 16474–16481.

62. J. D. Holbrey, W. M. Reichert, R. D. Rogers, *Dalton Trans*., 2004, 2267–2271.

63. J. N. C. Lopes, K. Shimizu, A. A. H. Pádua, Y. Umebayashi, S. Fukuda, K. Fujii, S. A. Ishiguro, *J. Phys. Chem. B*, 2008, **112**, 1465–1472.

64. P. Bonhôte, A. P. Dias, N. Papageorgiou, K. Kalyanasundaram, M. Grätzel, *Inorg. Chem*., 1996, **35**, 1168–1178.

65. P. Wasserscheid, T. Welton (Eds.), *Ionic Liquids in Synthesis,* Wiley-VCH, Weinheim, 2003.

66. L. Martin, E. Burello, P. N. Davey, K. R. Seddon, G. Rothenberg, *ChemPhysChem*, 2007, **8**, 690–695.

67. D. Holbrey, K. R. Seddon, *J. Chem. Soc., Dalton Trans*., 1999, 2133–2140.

68. K. Nishikawa, S. Wang, H. Katayanagi, S. Hayashi, H. Hamaguchi, Y. Koga, K. Tozaki, *J Phys. Chem B*, 2007, **111**, 4894–4900.

69. T. Mandai, H. Masu, H. Seki, K. Nishikawa, *Bull. Chem. Soc. Jpn*., 2012, **85**, 599–605.

70. S. Tsuzuki, T. Umecky, H. Matsumoto, W. Shinoda, M. Mikami, *J. Phys. Chem. B*, 2010, **114**, 11390–11396.

71. M. Yoshizawa, W. Xu, C. A. Angell, *J. Am. Chem. Soc*., 2003, **125**, 15411–15419.

72. S. Tsuzuki, W. Shinoda, S. Seki, Y. Umebayashi, K. Yoshida, K. Dokko, M. Watanabe, *ChemPhysChem*, 2013, **14**, 1993–2001.